




Verification of He-3 proportional counters' fast neutron sensitivity through a comparison with He-4 detectors

He-3 and He-4 proportional counters' fast neutron sensitivity and evaluation of the cosmic neutron fluxes at ESS

Francesco Piscitelli^{1,a} , Giacomo Mauri^{1,2}, Alessio Laloni¹, Richard Hall-Wilton^{1,3}

¹ European Spallation Source ERIC, P.O. Box 176, SE-221 00 Lund, Sweden

² Science and Technology Facilities Council, ISIS Department, Rutherford Appleton Labs, Didcot OX11 0QX, UK

³ Dipartimento di Fisica "G. Occhialini", University of Milano-Bicocca, Milan, Italy

Received: 21 February 2020 / Accepted: 8 July 2020 / Published online: 16 July 2020

© The Author(s) 2020

Abstract In the field of neutron scattering science, a large variety of instruments require detectors for thermal and cold neutrons. Helium-3 has been one of the main actors in thermal and cold neutron detection for many years. Nowadays, neutron facilities around the world are pushing their technologies to increase the available flux delivered at the instruments; this enables a completely new science landscape. Complementary with the increasing available flux, a better signal-to-background (S/B) ratio enables to perform new types of measurements. For instance, in neutron reflectometry, the time resolution for kinetic studies is limited by the available S/B. An improved S/B opens the possibility of sub-second kinetic studies. To this aim, this manuscript re-examines the background sensitivity of today's "gold standard" neutron detection. Fast neutrons and gamma rays are the main background species in neutron scattering experiments. The efficiency (sensitivity) of detecting fast neutrons, cosmic rays and gamma rays, for a Helium-3-based detector is studied here through the comparison with Helium-4 counters. The comparison with Helium-4 allows to separate the thermal (and cold) neutron from the fast neutron contributions in Helium-3-based counters which are otherwise entangled, verifying previous results from an indirect method. A relatively high sensitivity is found. Moreover, an estimate for the cosmic neutron fluence, also a source of background, at ground level at ESS is presented in this manuscript.

1 Introduction

Nowadays, neutron scattering facilities are increasing their available flux delivered at their instruments, which allows more complex scientific investigations and enables new science. The new generation of high-intensity neutron sources, such as the Japan Spallation Source (J-PARC [1]), the Spallation Neutron Source (SNS [2]) in the USA and the European Spallation Source (ESS [3–6]) presently under construction in Lund (Sweden), are able to provide, with respect to the previous generation sources, at least one order of magnitude higher flux delivered at the instruments [6–9]. Along with the gain of available and useful

^a e-mail: francesco.piscitelli@ess.eu (corresponding author)

neutron flux, an increase in background is expected. Therefore, a better signal-to-background (S/B) ratio is crucial to operate highly performing instruments. A scientific result depends on the S/B as a whole, a higher intensity of the source does not implicate a better result, and the improvement in the background is also essential.

The acceptance level of S/B is a property of the specific technique/instrument, and background identification is performed differently for different techniques. For example, in neutron specular reflectometry, the S/B is the ratio between the reflected intensity and any intensity integrated over the whole detector area outside the reflected intensity [10–12]. In inelastic (cold) neutron scattering, a vanadium sample is often used as an elastic scatterer and the S/B is the maximum in intensity at the elastic line compared to the generally flat background far away from the elastic peak [13].

Shielding material is employed to reduce the background at an instrument; however, heavy shielding components do not always represent a viable solution due to the limited space available and its high cost. Moreover, a background radiation is delivered through the same delivery system used to guide thermal, useful, neutrons to the instrument. Hence, in order to achieve a high S/B rejection, it is imperative to require a detector with high detection efficiency (at thermal and cold energies, ≈ 25 meV) and with a very low efficiency (sensitivity) to other types of radiation. A source of background in a neutron scattering facility is mainly due to gamma rays, epi-thermal, fast neutrons and cosmic rays [14]. When any of these radiations is detected, it results in spurious events recorded as “good” events. It is possible to identify background events only if a pulse analysis is performed that usually limits the counting rate at which the detector can be operated. Note that the electronic noise can be a further source of background.

The sensitivity, which is analytically defined as the efficiency, is the probability for an incident radiation on a detector element (a whole counter in the present work) to result into an event. Whereas the efficiency represents a valuable feature of a device, that is desirable to be as high as possible, the sensitivity is, instead, the efficiency of detecting an unwanted radiation. In the case of a thermal neutron detector, the efficiency is the probability of detecting a thermal neutron and its sensitivity is the probability of detecting fast neutrons or gamma rays. Together, the efficiency and the sensitivity define the best achievable S/B for a detector. Practically, if a portable source is used, the sensitivity is the number of events that exceed a set energy threshold in the pulse height spectrum (PHS), normalised to the activity of the source and the solid angle subtended by the detector element.

Although Helium-3 has been the main actor in neutron detection for decades, many alternative technologies [15–17] have been proposed and developed during the last ten years to face the challenge of the Helium-3 shortage and performance [16, 18–21]. The Helium-3 performance in terms of counting rate capability is not only an intrinsic property of the neutron converter medium on itself, but depends on the mechanical and read-out schemes used as well. For example, conversion volumes segmentation or an individual read-out scheme is preferred to a single volume and to a charge division read-out method. On the other hand, the spatial resolution and the sensitivity to background are peculiar features of the Helium-3 itself. Helium-3 still represents a valid neutron detection medium for scattering science for some applications. A valid alternative to Helium-3 is Boron-10 [22–24] used as a solid converter layer in detectors. The Multi-Grid [25–28] for large area applications in neutron spectroscopy, the Multi-Blade [29–35] for neutron reflectometry, the Jalousie detector [36, 37] for neutron diffraction, BandGEM [38, 39], the boron-coated straws [40–45] for SANS instruments, and CASCADE [46, 47] are some of the newly developed Boron-10-based detectors. Moreover, other converter materials have been also investigated as a replacement for Helium-3, as an

example gadolinium has been coupled to a gas electron multiplier (GEM [48]) device in the Gd-GEM detector [49, 50] or coupled to solid-state detectors [51–54].

It has been shown that Boron-10-based proportional counters or multi-wire proportional chambers (MWPC) can achieve a gamma-ray sensitivity as low as Helium-3-based detectors below 10^{-6} [32, 55].

Boron-10-based detectors' fast neutron sensitivity has been measured and simulated, and it is of the order of 10^{-5} [56].

An indirect method based on a series of measurements with different absorbers and simulations has indicated that Helium-3 has a fast neutron sensitivity of the order of 10^{-3} [57].

In this manuscript, a complementary method is presented. The sensitivity to fast neutrons and gamma rays of a Helium-3 counter is verified by comparing with a Helium-4 counter. These two isotopes have comparable cross sections to fast neutrons, whereas the Helium-4 can be considered insensitive to thermal neutrons, because of a much lower cross section with respect to the Helium-3. This allows to disentangle the sensitivity to fast neutrons from thermal neutrons. The theoretical considerations to support this assumption are outlined in the next section.

Note that epi-thermal neutrons also contribute to the background, but this contribution is not discussed in this manuscript. The fast neutron energy range is set by the available neutron sources at our laboratory, and it ranges between 1 and 10 MeV. Fast neutron background energy range in spallation sources is wider than this and can extend up to 100 MeV.

The results presented in this manuscript serve as a reference benchmark for detectors used in neutron scattering science; the measurements of the intrinsic sensitivity to a background radiation are presented. Note that the response of a detector in a background field can only be comprehensively performed in the actual experimental configuration.

Moreover, the measurement with cosmic rays, also a possible source of background, is shown here to verify the actual thermal and fast cosmic neutron fluxes present at the ground level at ESS.

2 Theoretical considerations

The sensitivity of gaseous detectors to fast neutrons is mainly given by the gaseous media, and very little contribution is observed from the solid materials of the detector [56]. In the case of Boron-10-based detectors, the neutron converting material can be easily removed from the detector to evaluate experimentally the detection of fast neutrons. On the other hand, in Helium-3 detectors the detection of thermal and cold neutrons cannot be disentangled from the detection of fast or epi-thermal neutrons. Simulations and indirect measurements have been performed on this matter [57].

Helium-3 is used as a means in fast neutron spectroscopy [58–60], whereas Helium-4 is employed for fast neutron detection [58, 61–65]. Due to its cross section (shown in Fig. 1), Helium-4 is not sensitive to thermal neutrons through a conversion process; hence, it gives an insight of the fast neutron sensitivity of Helium-3 at fast neutron energies. With Helium-4, the fast neutron sensitivity can be disentangled from the sensitivity to thermal and cold neutrons of Helium-3. The possible interactions that a neutron can undergo when interacting with Helium-3 and Helium-4 nuclei are listed here:

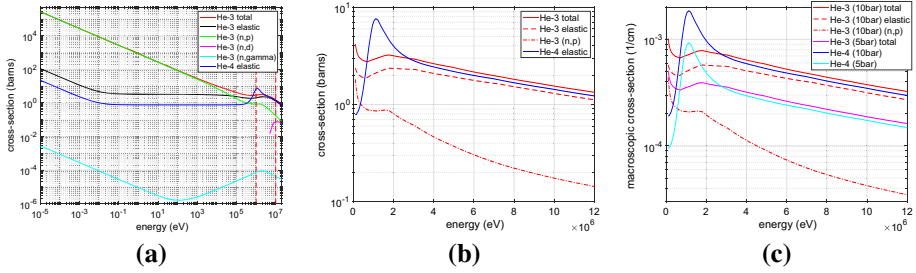
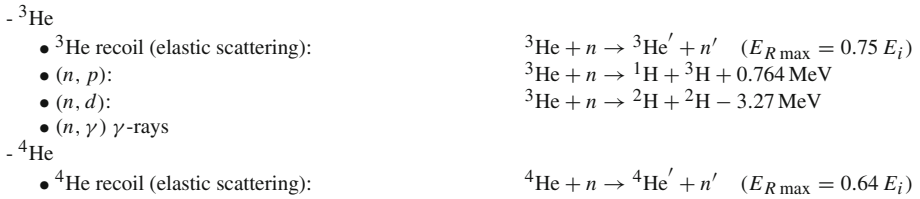


Fig. 1 **a** Cross section for various processes of a neutron interacting with either Helium-3 or Helium-4 nuclei. **b** Same as **a** in the neutron energy range 0–12 MeV. **c** Macroscopic cross sections for 5 and 10 bar of Helium-3 or Helium-4 in the energy range 0–12 MeV. From [66,67]



Helium-4, opposite to Helium-3, can interact with neutrons only via elastic scattering (recoil) in the whole energy range that spans from cold up to fast neutron energies. On the other hand, a neutron can be also captured (absorption interaction) or excite the target nucleus (inelastic interaction) when interacting with Helium-3. Figure 1 shows the cross sections of those processes, in the wide energy range from μeV up to MeV (a) and in the energy range $\approx 1\text{--}10$ MeV (b) of interest for this manuscript. Moreover, the macroscopic cross section is shown distinguishing between two gas pressure for each type of detector (c). The macroscopic cross section (Σ) is the probability that a neutron (in our specific case) will undergo a reaction per unit path length travelled in the material, and it is calculated as the product of the microscopic cross section σ and the number density. The macroscopic cross section is also known as the attenuation coefficient.

In the case of neutrons interacting with Helium-3, the (n, γ) process can be neglected being its cross section of several orders of magnitude smaller than any other possible reaction. The (n, d) reaction occurs at energies above ≈ 10 MeV. It can be neglected as well, since the source used for this investigation emits neutrons in the 1–10 MeV energy range and it is also two orders of magnitude smaller than the cross section of recoil (elastic interaction) and (n,p) (absorption) processes. Thus, only these two latter mechanisms are considered for the calculations regarding Helium-3.

In the 1–10 MeV range, the combination of absorption and recoil in Helium-3 sums up to a comparable cross section to the sole recoil cross section of Helium-4. The average total cross section in the considered energy range is 2.54 barns and 2.34 barns for Helium-4 and Helium-3, respectively; i.e. the probability of interaction with Helium-3 and Helium-4 is similar.

The gas pressure used in Helium-3-filled detectors is typically below 20 bar. Below this pressure, the ideal gas approximation holds and it can be used to evaluate the number density of the gas given its partial pressure. The number density, in this approximation, also scales

linearly with the partial pressure. Thus, the number density does not depend on the type of gas, and it is $2.4 \cdot 10^{19} \text{ cm}^{-3}$ (at 1 bar) for either Helium-3 or Helium-4. On the other hand, the mass density of the two gases differs and this impacts the way a helium ion releases its energy into the gas volume. The mass density is $1.2 \cdot 10^{-4} \text{ g/cm}^3$ and $1.6 \cdot 10^{-4} \text{ g/cm}^3$ at 1 bar for Helium-3 and Helium-4, respectively.

Figure 1c shows the macroscopic cross section (Σ) for the two gases at the pressures of 5 and 10 bar. The macroscopic cross section represents the probability, per unit length, of interaction of a neutron with the nucleus under consideration. For small values of $\Sigma \cdot x$, the interaction probability can be approximated as:

$$P(x) = 1 - e^{-\Sigma \cdot x} \approx \Sigma \cdot x. \quad (1)$$

Therefore, the plot in Fig. 1c represents also the probability per unit length ($P(x)/x$) of having an interaction with any of the two nuclei for a given pressure, 5 and 10 bar in this specific case. At fixed partial pressure (e.g. at 10 bar), the interaction probability (given by the total cross section) for Helium-3 and Helium-4 can be considered similar and of the order of $10^{-4} - 10^{-3}/\text{cm}$. For instance, for a 2.54-cm-diameter tube filled with 10 bar helium, the probability of interaction is simply 2.54 times higher.

In the case of an elastic interaction, either for Helium-3 or Helium-4, the maximum energy that the recoiled nucleus can receive in the interaction is given by Eq. 2:

$$E_{R \max} = \frac{4A}{(1+A)^2} E_i \quad (2)$$

where A is the mass number of the isotope.

Helium-3 detectors are used in fast neutron spectroscopy measurements [58–60], because in the case of a mono-energetic fast neutron beam, the incoming neutrons energy can be deduced. Let us consider an ideal detector case, where the wall effect can be neglected, and a beam of mono-energetic E_i incoming neutrons. In the case of Helium-4, the cross section is totally elastic and only recoil occurs. From Eq. 2, the maximum energy transferred is $E_{R \max} = 0.64 \cdot E_i$. This gives a continuous distribution in the pulse height spectrum (PHS) which spans from zero up to $E_{R \max}$. Figure 2 shows a sketch of a possible PHS obtained with a mono-energetic neutron beam for both isotopes. In the case of Helium-3, the absorption cross section (n, p) gives rise to a peak in the PHS at the energy $E_i + Q$, where Q is the Q value for the neutron capture reaction which is $Q = 0.764 \text{ MeV}$. The elastic cross section contributes to a recoil distribution in the PHS which extends up to $E_{R \max} = 0.75 \cdot E_i$.

If thermal and epi-thermal neutrons are also present, they both give rise to the characteristic peak at energy Q in the PHS due to the Helium-3 capture reaction. Thermal and epi-thermal neutrons cannot be distinguished in the PHS. At energies below $\approx 10^4 \text{ eV}$, the absorption cross section exceeds the elastic cross sections and the absorption process becomes much more probable than recoil. Therefore, the peak at energy Q becomes predominant at these energies [58].

If a neutron source is used, the incoming energy distribution is far from being mono-energetic and, along with fast, also thermal and epi-thermal neutrons will be present due to the moderation processes happening in the surroundings of the detector. The PHS for Helium-3 in this case will be the superposition of three components: the characteristic peak at energy Q due to thermal and epi-thermal neutrons, the summation of many recoil events each with maximum energy $E_{R \max}$ and the overlap of many capture events each with energy $E_i + Q$. Thus, no peak at $E_i + Q$ can be identified any more. On the other hand, for Helium-4 the PHS will be a simple continuum obtained by the summation of the several events given by the recoiled nuclei, each with maximum energy $E_{R \max}$.

Fig. 2 Theoretical sketch of the PHS obtained with a counter (neglecting wall effects) filled with Helium-3 or Helium-4 when exposed to a mono-energetic E_i fast neutron beam

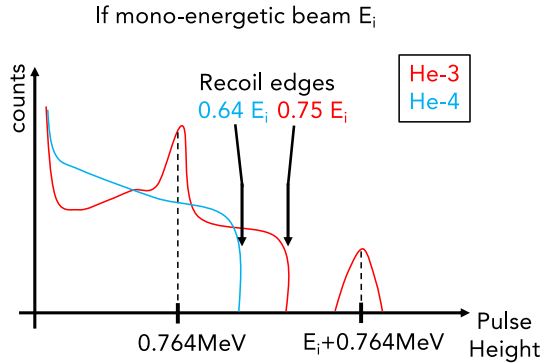


Table 1 Ranges of recoil nuclei for 100 keV energy threshold and 1 bar. Relative uncertainties never exceed 3%

Energy (MeV)	Range (cm) ${}^3\text{He}^{++}$ in ${}^3\text{He}$	Range (cm) ${}^4\text{He}^{++}$ in ${}^4\text{He}$
1	2.14	2.39
2	4.61	5.03
3	8.09	8.55
4	12.52	12.98
5	17.89	18.29
6	24.16	24.47
7	31.27	31.49
8	39.25	39.34
9	48.06	47.96
10	57.60	57.29

Moreover, in a real detector case, a detector has a finite pressure and volume which introduces the wall effect in the PHS.

Once a nucleus recoils, it loses energy according to the Bethe–Bloch formula [58]. The stopping power of a ${}^3\text{He}^{++}$ ion in Helium-3 or ${}^4\text{He}^{++}$ ion in Helium-4 for a given pressure and incoming energy can be calculated with SRIM [68,69]. The stopping power allows to extrapolate the range of those particles in the gas and the amount of energy that can be deposited in a given volume. Table 1 shows the ranges for several energies for both Helium-3 and Helium-4 ions for 1 bar pressure. These values scale linearly inverse with the pressure.

Although the mass density of the two gases differs, the ranges of the recoiled nuclei are similar.

The maximum energy that can be released in the gas can be calculated, from the stopping power, for different thicknesses of the gas volume and pressures. In the case of a gas volume large enough so that the ion is fully stopped, the dependency between the energy released by a nucleus and its recoiling energy is linear. Figure 3 shows the relationship between the recoiling energy and the released energy for three different thickness of the gas volume (1 cm, 2.54 cm and 10 cm) and three different pressures of the gases (1, 5 and 10 bar).

Given that the ranges in the two media are similar, it is clear that for a given volume and pressure, the energy deposition in the gas for the two isotopes follows the same behaviour.

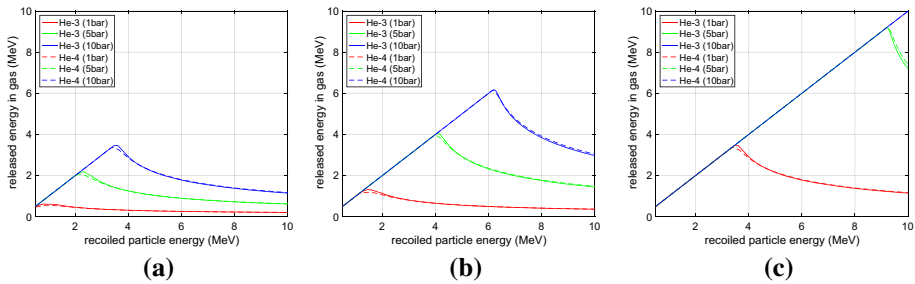


Fig. 3 Released energy of ions (${}^3\text{He}^{++}$ in ${}^3\text{He}$ and ${}^4\text{He}^{++}$ in ${}^4\text{He}$) as a function of the energy gained after recoiling for 1, 5 and 10 bar and **a** 1 cm gas depth, **b** 2.54 cm and **c** 10 cm

To conclude, the two isotopes, for a given volume, pressure and detector geometry, behave similarly: they show a comparable average total cross section in the range 1–10 MeV, the interaction of a fast neutron with Helium-3 or Helium-4 has a similar probability to occur, and the energy released for a recoiled ion, with given energy, is almost identical. The range of a ${}^4\text{He}^{++}$ ions in Helium-4 is similar to the range of a ${}^3\text{He}^{++}$ ion in Helium-3. The only difference between the two isotopes is the maximum energy that the recoiled nucleus can receive from an impact (E_{Rmax}).

Based on this assumption, the sensitivity of Helium-3 to fast neutrons is, on the order of magnitude accuracy, equal to the sensitivity of Helium-4 multiplied by the ratio between the two maximum recoil energies (Eq. 2). Namely, the energy axis of the Helium-4 PHS has to be shifted by the quantity $\frac{0.75}{0.64} = 1.17$. This shift is needed if a non-mono-energetic source of fast neutrons is used; with a mono-energetic beam, the same average recoil energy can be achieved using a 1.17 times more energetic beam for the Helium-4 with respect to that of the Helium 3.

For a given incoming distribution of neutron energies, the PHSs of Helium-3 and Helium-4 (even if shifted) will not only differ for energies below $Q = 0.764$ MeV, where thermal and epi-thermal neutrons contribute to the spectrum, but also above such energy, where the contribution is only given by fast neutrons in both detectors. Assuming an identical total macroscopic cross section for both isotopes, the Helium-4 cross section is entirely given by the elastic process, whereas that of Helium-3 is given, on average, to the absorption and to the elastic cross section by 1/5 and 4/5, respectively. The absorption process is responsible of generating events in the PHS at the energies $E_i + Q$ with all possible E_i . This will raise the PHS of Helium-3 at energies above $Q = 0.764$ MeV by approximately 1/5. This effect will be discussed in Sect. 3.2.

Nevertheless, the overall sensitivity of Helium-4 is a good indication of the sensitivity of Helium-3 because in order to calculate the sensitivity, only the PHS integral (above a given energy threshold) matters.

3 Measurements

3.1 Experimental set-up

Three proportional counters have been used: two Helium-4 tubes, by Toshiba/Canon Electron Tubes & Devices Co. Ltd. [70], with partial pressure of 10 and 5 bar, respectively, and a Helium-3 tube, by General Electric (GE) [71], with partial pressure of 10 bar (Fig. 4). In

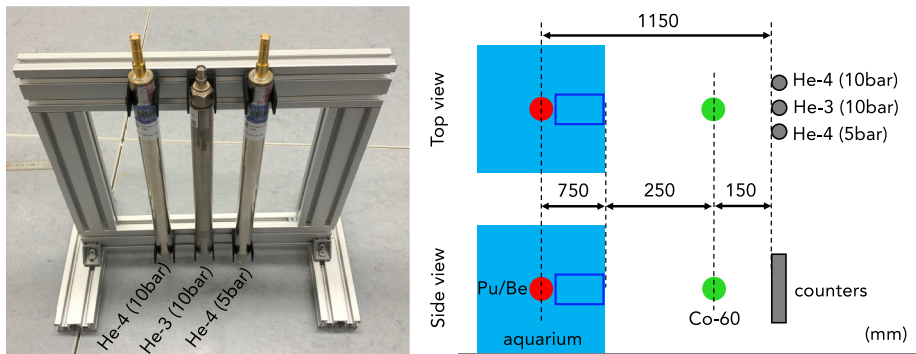


Fig. 4 Photograph of the stand supporting the three counters used in the measurements (left). Sketch of the experimental set-up (right). Dimensions are in mm

addition to helium, in each of the three tubes there is also a small amount (≈ 0.15 bar) of CO_2 . All tubes have an active length of approximately 25 cm and a diameter of 2.54 cm. The detector wall is made of stainless steel, and it is 0.05 cm thick for all tubes.

The efficiency to thermal neutrons of the Helium-3 tube can be calculated according to its pressure, and it has also been measured with a mono-energetic neutron beam of 2.5\AA , resulting into a detection efficiency of $\approx 96\%$. This value agrees with the calculation within 2% uncertainty.

The tubes have been placed side by side and exposed to the same flux (Fig. 4); the measurements have been carried out simultaneously with the three tubes. Each tube is connected to a CREMAT [72] charge amplifier and shaping amplifier in sequence, with overall gain of 14 V/pC and $1\ \mu\text{s}$ shaping time. The analogue output of each amplifier is connected to a single channel of a CAEN V1740D digitiser (12 bit, 62.5MS/s) [73]. The digitiser is equipped with a DPP-QDC (digital pulse processing) firmware; only a value (QDC) proportional to the energy released in each counter is recorded and not the full signal trace. Note that the signals are shaped in time; hence, any value among amplitude, pulse integral (QDC) or time-over-threshold (ToT) gives the same information: a value proportional to the energy released in the counter that can be used to build the pulse height spectrum (PHS).

The counters have been firstly characterised with cosmic neutrons. These measurement have been carried out at the ESS laboratory Utgård in Lund (SE). The measurements with the sources have been performed at the Source Testing Facility (STF) [74,75] at the Lund University in Lund (SE). This user facility is equipped with a complete range of neutron and gamma-ray sources for the characterisation of detectors. In particular, the measurements presented in this manuscript have been performed by using the so-called *Aquarium* available at the STF.

The Aquarium is a custom-designed shielding apparatus for neutron sources, delivering neutron beams at each cavity of this structure. The Aquarium consists of a cube of Plexiglas (≈ 1.4 m side), filled with about 2650 litres of high-purity water. A neutron source can be placed in its centre. Four horizontal cylindrical apertures of approximately 17 cm diameter are perpendicular to each of the four vertical faces of the cube, providing four uniform combined beams of gamma rays and neutrons from the source. A sketch of the set-up is shown in Fig. 4.

The use of the Aquarium, instead of a bare source, has the effect of decreasing the neutron background detected by the counters. The neutrons that are not exiting the Aquarium through one of its ports are absorbed by the large amount of water that surrounds the source. Moreover,

the tubes are covered with a 2-mm-thick Mirrobor sheet (only the side of each tube facing the beam port is left uncovered) to further decrease the background neutrons that are scattered by the surrounding environment back into the counters.

Two sources have been used in the measurements: a $^{238}\text{Pu}/^9\text{Be}$ (Pu/Be) source of certified activity and neutron yield [76] and a Co-60 gamma-ray source of 9×10^6 Bq.

The gamma-ray source was used in order to have a comparison with the previous work on gamma-ray sensitivity of Boron-10 and Helium-3 detectors [32,55–57]. Co-60 mainly emits gamma rays at 1.173 MeV and 1.332 MeV with unitary intensity; any other emitted gamma ray can be neglected for our purposes because of their weak intensity.

The Pu/Be source has been previously characterised [77], and its neutron emission spectrum, nearly isotropic, ranges from approximately 1 to 10 MeV, with a most probable energy of 3 MeV [77,78].

3.2 Results and discussion

3.2.1 Cosmic neutron fluxes at ground level at ESS

Neutrons are created through the process of cosmic ray spallation when high-energy particles collide with atmospheric nuclei. They penetrate much further into atmosphere than the electromagnetic radiations as they are not geomagnetically trapped [79]. Cosmic neutrons undergo a slowing down process in the atmosphere that brings a part of them to thermal energies (appropriately 25 meV); thus, neutrons with a very wide energy distribution, spanning from thermal to fast energies, reach the ground level. Those neutrons cannot be distinguished from thermal and fast neutrons generated at the neutron facility. This section provides an estimate of the flux of cosmic neutrons at the ground level at ESS is given. These figures can be used in the future to quantify any background generated from cosmic neutrons at ESS.

Two measurements have been performed simultaneously with the three tubes, one with the bare tubes (C) and one with the tubes fully covered with a 2-mm Mirrobor sheets as a thermal and cold neutron absorber (S). Figure 5 shows the PHS, normalised by time, for the three counters in the two configurations.

The typical spectrum for a Helium-3 counter apart from the peak at $Q = 0.764$ MeV has a step structure due to the wall effect [58], where the proton (570 keV) and triton (190 keV) energies can be identified. A sharp drop in the spectrum is expected, and it extends down to low energies. (A further peak due to the gamma rays occurs at very low energies.) The presence of thermal neutrons in the incoming cosmic flux can be verified by the measurement in configuration (S). Indeed, the Mirrobor mainly absorbs thermal neutrons while keeping the fast neutron flux unaltered.

The horizontal axis of the PHS has been converted into energy (keV) from arbitrary channels (QDCs) by using the centre of the peak of the Helium-3 absorption process corresponding to an energy of $Q = 0.764$ MeV. The hardware threshold in the CAEN system has been set in order to reject the electronic noise, and it corresponds to approximately 80 keV. Each PHS has no sharp cut at low energies, but it extends up to zero. This is due to the DPP-QDC firmware used. When the amplitude of the pulses is close to the hardware threshold used to reject noise, the area of such pulses, calculated by the firmware, is affected by a very high uncertainty. If, instead, the amplitudes of the pulses were recorded, no values below the set threshold would appear in the PHS. The characteristic Helium-3 PHS is highly attenuated in the configuration (S), meaning that the neutrons reaching the Helium-3 counter are efficiently stopped by the Mirrobor sheet. Due to the imperfection of the electronics chain, the Helium-4 tube at 5 bar shows a higher noise with respect to the others.

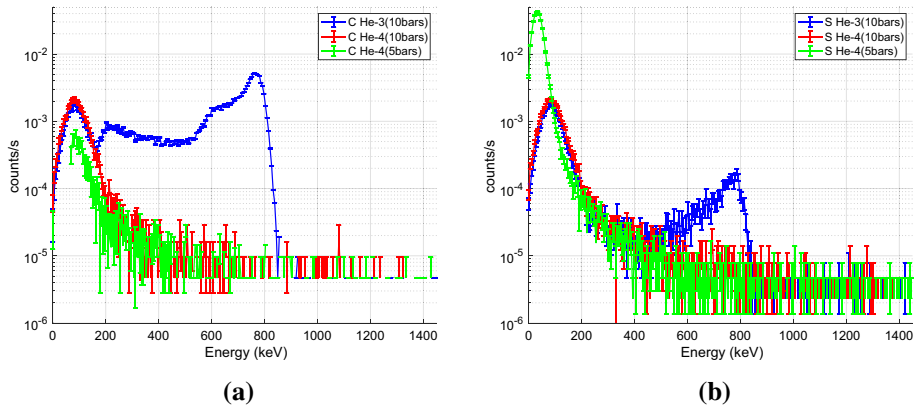


Fig. 5 **a** PHS for the three counters in the configuration (C) with the tubes fully exposed. **b** PHS for the three counters in the configuration (S) with the tubes covered with a 2-mm-thick Mirrobor sheet. The PHS is normalised by the time of the measurements

Table 2 Rates recorded by the three counters in three configurations and two values for the energy threshold. The rates are shown for both the configurations (C) and (S) and when no high voltage (HV) is applied to the counters in order to evaluate the electronics noise. The relative uncertainty is approximately 40% for the data without HV, and it never exceeds 3% for the configurations (C) and (S)

Threshold (keV)	Detector	No HV	No shield (C)	Shield (S)	
80	He-3 (10 bar)	$1.59 \cdot 10^{-4}$	0.174	0.032	Hz
	He-4 (10 bar)	$1.49 \cdot 10^{-4}$	0.035	0.037	Hz
	He-4 (5 bar)	0.121	0.111	0.470	Hz
150	He-3 (10 bar)	$6.94 \cdot 10^{-5}$	0.148	$7.13 \cdot 10^{-3}$	Hz
	He-4 (10 bar)	$6.94 \cdot 10^{-5}$	$4.29 \cdot 10^{-3}$	$5.28 \cdot 10^{-3}$	Hz
	He-4 (5 bar)	$1.89 \cdot 10^{-3}$	$4.02 \cdot 10^{-3}$	0.015	Hz

Table 2 shows the total number of counts, for each detector, by summing the PHS from a given threshold up to the maximum energy in the spectrum. The PHS integral is shown for 80 keV and for 150 keV which is the threshold generally chosen for a Helium-3 counter in normal operation to reject gamma rays. In order to evaluate the amount of electronic noise above the set threshold, a set of measurements have been performed without applying the high voltage (HV) to the counters.

Cosmic neutron rates have been measured elsewhere by the Physikalisch-Technische Bundesanstalt (PTB) through the use of an extended-range Bonner sphere spectrometer [80]. The neutron fluence rates (integrated over the total energy range from 10^{-9} to 10^3 MeV) are given for three different elevations, and at 85 m over the sea level (similarly to the elevation of Lund, Sweden), the rate is about 135 Hz/m^2 [81, 82]. In order to compare with the results shown here, the rates in Table 2 have to be normalised by the area or volume of the detectors. Table 3 shows the rates recorded with the two 10 bar counters, in configurations (C) and (S), with the 150 keV threshold. Normalisation by the side area ($6.3 \cdot 10^{-3} \text{ m}^2$) and volume ($5.07 \cdot 10^{-4} \text{ m}^3$) of the tube is applied. The side area of a tube is the area obtained by the product of the tube diameter and its active length. Generally, in neutron scattering science, the instruments have detector arrays comprised of many of such tubes. The side area of each

Table 3 Rates for the two 10 bar counters with 150 keV threshold applied recorded in configuration (C) and (S) and normalised by the side area of the tube ($6.3 \cdot 10^{-3} \text{ m}^2$) and by their volume ($5.07 \cdot 10^{-4} \text{ m}^3$)

Detector	Rate per tube (Hz)		Rate per area (Hz/m^2)		Rate per volume (Hz/m^3)	
	No shield (C)	Shield (S)	No shield (C)	Shield (S)	No shield (C)	Shield (S)
He-3 (10 bar)	0.148	$7.13 \cdot 10^{-3}$	23.3	1.13	292.1	14.1
He-4 (10 bar)	$4.29 \cdot 10^{-3}$	$5.28 \cdot 10^{-3}$	0.676	0.84	8.47	10.4

tube is orthogonal to the neutron beam incoming direction, and for this reason the side area is taken in the normalisation.

For the tubes filled with 10 bar, a thermal cosmic neutron flux of about 0.029 Hz/(bar·litre) of Helium-3 is expected without shielding and of about 0.0014 Hz/(bar·litre) with shielding. These rates are in agreement with cosmic rates measured at the FRM-II reactor [83]. They are also compatible with the measurements carried out by PTB [81, 82] of 135 Hz/m². One has to consider that the Helium-3 counter is mainly sensitive to the thermal neutrons as it would be a Bonner sphere spectrometer used without any polyethylene moderator. On the other hand, the Helium-4 detector would be as a Bonner sphere more sensitive to fast neutrons with a very low efficiency. Hence, the rate presented here represents only a fraction of the spectrum measured by PTB.

In the case of a neutron scattering experiment, the proportional counters are stacked in an array. The figures extrapolated for a single tube, for either a shielded detector or a bare detector, represent an upper limit for the detected cosmic neutron events. In a stacking configuration, each counter acts as shielding on its own neighbours, reducing the amount of cosmic neutrons that reach a particular counter.

The imperfection of the manufacture of the counters introduces an extra uncertainty on the detectors' gain, consequently on the energy thresholds, across the tubes. Thus, the cosmic neutron background measured here only represents an order of magnitude of the neutron fluence at ESS to which neutron scattering detectors are exposed.

3.2.2 Fast neutron sensitivity of He-3 and He-4 counters

In this section, an order of magnitude for the absolute fast neutron sensitivity of a Helium-3 counter is obtained by comparing with a Helium-4 detector. Three measurements have been carried out with the three counters used simultaneously: a background measurement (B), a measurement with the Pu/Be source (fast neutrons—N) and a measurement with a Co-60 source (gamma rays—G). In the tables and plot, the three configurations are also referred as: n for neutrons (N), γ for gamma rays (G) and bg for background (B).

The background (B) has been estimated by removing all radioactive sources from the experimental area. Neutrons are very complicated to shield, and for this reason the Pu/Be source has been taken in a separate laboratory area not to influence the background measurement. Figure 6 shows the PHS recorded in the three configurations (B, N, G) with the three counters. The uncertainty bars in the plot represent the Poissonian uncertainty due to the counting statistics.

The horizontal axis of the PHS has been converted into energy as explained in the previous section. The acquisition system has an input dynamic range limited between 0 and 2 volts; thus, every event with larger amplitude is recorded with the same value indifferently from the real charge deposited. These overflow events are shown in the last bin of the histogram

Fig. 6 PHS recorded with the three counters in the three different measurements: B (bg—background with no sources), N (n—Pu/Be) and G (γ —gamma rays). The PHS is normalised by the relative duration of the measurement

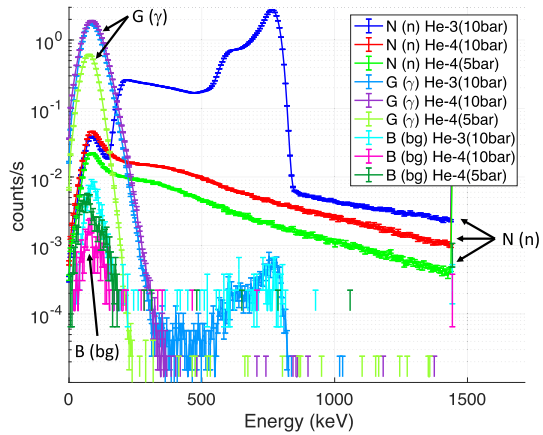


Table 4 Rates recorded by the three counters in three measurements: background, fast neutrons (Pu/Be) and gamma rays (Co-60). The recorded rates are all events that trigger the CAEN digitiser with a set hardware threshold which corresponds to approximately 80 keV normalised to the duration of the relative measurement

Detector	No sources (B - bg)	Pu/Be (N - n)	Co-60 (G - γ)	
He-3 (10 bar)	0.086	70	25	Hz
He-4 (10 bar)	0.021	2.2	30	Hz
He-4 (5 bar)	0.064	1.1	7.5	Hz

(at an energy of approximately 1450 keV). A Gaussian function is used to fit the full energy deposition peak from the neutron capture reaction at $Q=0.764$ MeV. The full width half maximum (FWHM) of such a function gives the energy resolution of the counter, and it is approximately 60 keV. Thus, any nucleus that recoils with an energy below this resolution cannot be distinguished from any other neutron which is instead captured.

By comparing the PHS recorded with the gamma source (G), Fig. 6, it can be noticed that the Helium-3 tube shows the characteristic neutron capture spectrum from energies between ≈ 400 and 800 keV. Although the neutron source was removed from the experimental area, some neutron can still reach the experimental set-up generating these events, which are less than $\approx 0.4\%$ of the total counts in the PHS.

Table 4 shows the rates recorded with the three tubes in the three different measurements when no further software threshold is applied to the PHS.

By comparing the rates in Table 4, the background affects the other measurements by no more than 5 %.

The greatest uncertainty comes from the measurement of the distance between the source and the detectors. We estimate that this can lead to the uncertainty of no more than a factor 2. The encapsulation of the Pu/Be is not the same as that of Co-60. The Co-60 can be considered a point-like source, whereas the Pu/Be core has a diameter of approximately 1 cm. For this reason, the Co-60 source was placed closer to the detector than the Pu/Be, at 15 cm subtending a solid angle of 0.23 str. The Pu/Be source was placed in the Aquarium at a distance of 115 cm from the detector, subtending a solid angle of 0.005 str. At this distance, the uncertainty due to the extension of the source is kept below 1% ($\frac{1 \text{ cm}}{115 \text{ cm}}$). Moreover, as mentioned above, the Aquarium reduces further the background from scattered and thermalised neutrons.

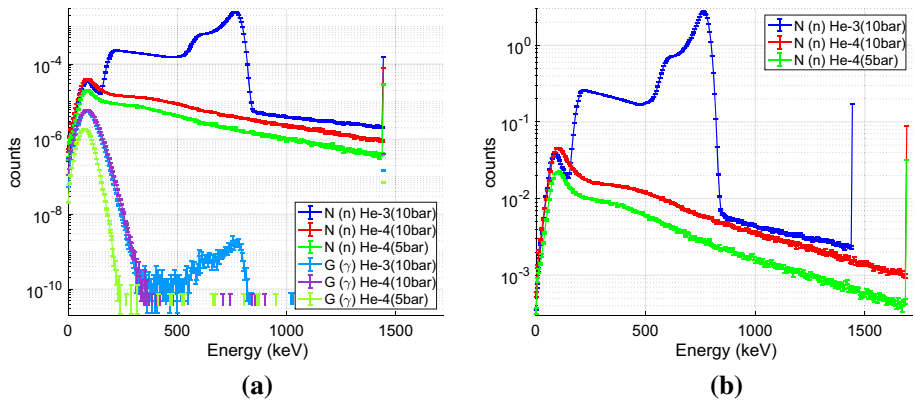


Fig. 7 **a** PHS of the three counters in the configurations N (n—Pu/Be) and G (γ —Co-60) normalised by the duration of the measurement, solid angle subtended by the source and its activity. **b** PHS of the three counters in the configuration N also normalised and the horizontal axis of the PHS belonging to the Helium-4 detectors also shifted by the ratio $\frac{0.75}{0.64} = 1.17$

All figures are given here with their associated Poissonian uncertainty due to the counting statistics. Further uncertainties derive from the placement of the sources (a factor 2) and background ($\leq 5\%$). This does not affect the aim of this work since only an order of magnitude for the fast neutron sensitivity is extracted.

The sensitivity is the ratio between the detected events, above a certain energy threshold, and the total number of impinging particles on the detector. The PHS has to be normalised by the duration of the measurement, the solid angle subtended by the source and by the number of emitted particles by the source in 4π and unit time (proportional to the activity of the source). Figure 7a shows the normalised PHS for the two configurations N and G.

As described in Sect. 2, in order to extrapolate the sensitivity of the Helium-3 counter, the horizontal axis of the PHS corresponding to the Helium-4 detectors has to be shifted by the ratio $\frac{0.75}{0.64} = 1.17$ to account for the different recoiling energy gained by the two isotopes. This is shown in Fig. 7b. Note that the PHS of the Helium-3 detector, for energies above the full energy deposition peak $Q = 0.764$ MeV, is approximately 1/5 higher than that of the Helium-4 detector (10 bar); this is in agreement with the theoretical considerations discussed in Sect. 2.

Figure 8 shows the sensitivity as a function of the energy threshold for each tube and for the two configurations N and G. This plot is obtained by summing all counts from a given value of the threshold up to the highest energy in the PHS. The sensitivities are also reported, in Table 5, for the values of threshold usually set in normal operation of the counters: 100, 150, 200 and 250 keV. The figures in Fig. 8 and Table 5 are shown with their associated statistical uncertainties; the uncertainties due to the background (5%) and the geometry of the set-up (a factor 2) have to be considered as well when comparing these figures.

The gamma-ray sensitivity (G) is in agreement with previous works on this matter [32,55,56]. It can be strongly suppressed by increasing slightly the energy threshold used. The Helium-3 and Helium-4 tubes, at a given pressure (10 bar), have the same gamma-ray sensitivity within the discussed uncertainties. It is very important to properly set the threshold in a neutron experiment because, as for Boron-10 detectors [55], the gamma-ray sensitivity of a Helium-3 detector scales by orders of magnitude in a very narrow range of the threshold. It is not always possible to identify the “valley” cut-off (at the triton (190 keV)

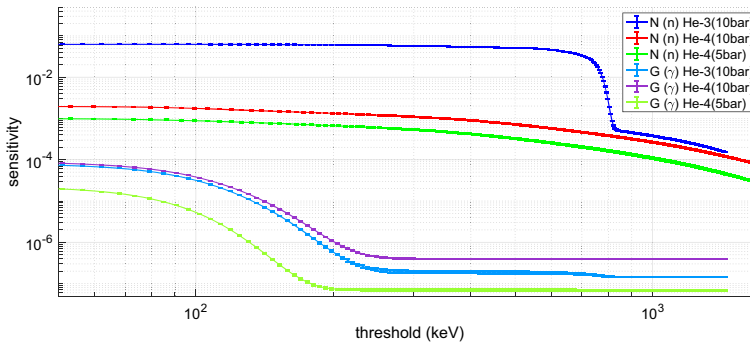


Fig. 8 Fast neutron and gamma-ray sensitivity of the three counters as a function of the energy threshold applied to their PHS

Table 5 Sensitivities for the three counters for the configurations N (n—Pu/Be) and G (γ —Co-60). Statistical uncertainties are reported as well. In addition to the Poissonian uncertainty, all figures have systematic uncertainties of a factor 2 due to the precision in the geometrical positioning of the source with respect to the tubes and 5 % due to the counts due to the environmental background. The sensitivity to fast neutrons (N) of the Helium-3 tube is shown in brackets; it includes thermal and epi-thermal neutron contributions

Threshold (keV)	Detector	Sensitivity N (n—Pu/Be) ($\times 10^{-3}$)	Sensitivity G (γ —Co-60) ($\times 10^{-6}$)
100	He-3 (10 bar)	(62.15 \pm 0.01)	30.13 \pm 0.03
	He-4 (10 bar)	1.721 \pm 0.002	36.44 \pm 0.04
	He-4 (5 bar)	0.867 \pm 0.001	0.488 \pm 0.01
150	He-3 (10 bar)	(61.95 \pm 0.01)	4.32 \pm 0.01
	He-4 (10 bar)	1.482 \pm 0.002	6.28 \pm 0.02
	He-4 (5 bar)	0.751 \pm 0.001	0.280 \pm 0.003
200	He-3 (10 bar)	(61.10 \pm 0.01)	0.508 \pm 0.004
	He-4 (10 bar)	1.315 \pm 0.002	0.941 \pm 0.006
	He-4 (5 bar)	0.662 \pm 0.001	0.073 \pm 0.001
250	He-3 (10 bar)	(59.07 \pm 0.01)	0.210 \pm 0.003
	He-4 (10 bar)	1.203 \pm 0.002	0.433 \pm 0.004
	He-4 (5 bar)	0.598 \pm 0.001	0.070 \pm 0.001

escape shoulder) in the Helium-3 PHS, and consequently the choice of the threshold becomes more difficult. This is mainly true when a charge division read-out scheme or higher pressure is used for Helium-3 detectors.

The sensitivity to fast neutrons (N) of the Helium-3 detector, in Table 5, is shown in brackets because it does not represent the actual tube sensitivity to fast neutrons since it is not possible to disentangle the thermal and epi-thermal contributions.

By comparing the 5 bar and 10 bar tubes, the sensitivity to fast neutrons (for a given threshold) scales linearly with the gas pressure as expected. Half pressure of Helium-4 in a counter results in about half sensitivity of the detector. For instance, the sensitivity, for 150 keV threshold, is approximately $3 \cdot 10^{-4}$ per bar · litre.

The Helium-4 detector at 10 bar indicates the sensitivity of the Helium-3 counter for the same gas pressure, and it is of the order of 10^{-3} . This result is in agreement with both the simulations and experimental results carried out in [57].

In an instrumental environment, a detector is exposed to a mixed field of radiation; gamma-ray and fast neutron fields can easily exceed by orders of magnitude the thermal or cold neutron flux that is relevant for the experiment. For instance, in the case of a neutron scattering experiment with a required background rejection below 1 %, the absolute gamma-ray flux impinging on the detector must not exceed 10^4 gamma rays per thermal neutron detected, while the fast neutron flux must be below 10^1 for a Helium-3-based detector.

It has been shown that Boron-10-based detectors have a similar gamma-ray sensitivity [32,55] of Helium-3-based detectors, but about 100 times lower fast neutron sensitivity (10^{-5}) [56,57]. Thus, for a single thermal neutron detected they can tolerate a fast neutron flux of 10^3 while keeping the same background rejection level (below 1 %).

4 Conclusions

New science is enabled by more powerful instruments at neutron sources that are increasing the available neutron flux delivered at the instruments. Higher flux may implicate higher background as well, mostly when heavy shielding is not a viable option due to space limitations. Along with a higher detector performance, such as better spatial resolution and counting rate capability, the signal-to-background (S/B) is a key feature that requires attention to enable the new investigations. Gamma rays and fast neutrons are the main species of background in a neutron scattering facility, and the flux on a detector of such radiations can easily exceed the thermal (and/or cold) neutron flux which carries the scientific information. Thus, improving the background rejection for a detector is as crucial as increasing the available flux at the instrument. Cosmic neutrons are an additional source of background that here has been quantified.

Cosmic neutron energies span a very wide energy range, and, when thermalised, they are detected with high efficiency resulting into events that are impossible to distinguish from thermal neutron from the instrument. A fluence of approximately 23 Hz/m^2 has been found with a bare Helium-3 counter and of about 1 Hz/m^2 if covered with a neutron absorber such as Mirrobor. This gives a fluence of about $0.029 \text{ Hz}/(\text{bar} \cdot \text{litre})$ without shielding and of about $0.0014 \text{ Hz}/(\text{bar} \cdot \text{litre})$ with shielding. Note that these figures represent an upper limit for the cosmic neutron flux because, in an actual detector array arrangement, the counters partly screen each other from this radiation.

Although many detector technologies have been developed to face the new challenges in the past ten years, Helium-3 is still a valid means of detection for some applications. The fast neutron sensitivity of a Helium-3 proportional counter has been verified here through the direct comparison with a Helium-4 detector. In a Helium-3 detector, it is not possible to directly disentangle the detection of thermal (and cold) neutrons from the detection of fast neutrons without a subtraction method. Therefore, the Helium-4 detector, with identical physical features, was used to measure the sole detection of fast neutrons. In this work, the fast neutron sensitivity has been studied between 1 and 10 MeV.

The fast neutron sensitivity is of the order of 10^{-3} (at 10 bar, 2.54 cm diameter), and this result agrees with a previous work which includes simulations and indirect measurements obtained with a subtraction method [57]. As expected, the sensitivity to fast neutrons, of approximately $3 \cdot 10^{-4}$ per bar · litre of Helium-3, scales linearly with the gas pressure.

The gamma-ray sensitivity has been measured as well, and the results agree with the previous works [32,55,56]; it is on the order of 10^{-6} , and it scales steeply in a very narrow range of the threshold. It is not always possible to identify the “valley” cut-off (190 keV) in the Helium-3 PHS, mainly when the counters are read-out with a charge division method, or a higher pressure of Helium-3 is used, and consequently the choice of the threshold becomes more difficult and crucial.

It has been shown that Boron-10-based detectors have a comparable gamma-ray sensitivity [32,55] than that of Helium-3-based detectors, but about 100 times lower fast neutron sensitivity (10^{-5}) [56,57].

When a detector is deployed at an instrument, it is exposed to a mixed field of radiation: fast neutron and gamma-ray fluxes can easily exceed the thermal and cold neutron fluxes carrying the scientific information. For a given instrument configuration and a fixed S/B, a Boron-10-based and a Helium-3-based detector can tolerate the same gamma-ray background, but a Boron-10 detector can stand 100 times higher fast neutron background than Helium-3-based detectors.

Acknowledgements This work was partially supported by the BrightnESS project, Work Package (WP) 4.2 (EU Horizon 2020, INFRADEV-3-2015, 676548) and carried out as a part of the collaboration between the European Spallation Source (Sweden) and the Lund University (Sweden). The work has been carried out at the Source Testing Facility at the Lund University (Sweden). The authors would like to thank Toshiba/Canon Electron Tubes & Devices Co. Ltd. for their collaboration and for providing the Helium-4 tubes used in this investigation.

Data Availability Statement The raw data (doi: 10.6084/m9.figshare.11876292.v1) relative to the measurements described in this manuscript can be downloaded from <https://doi.org/10.6084/m9.figshare.11876292.v1>

Open Access This article is licensed under a Creative Commons Attribution 4.0 International License, which permits use, sharing, adaptation, distribution and reproduction in any medium or format, as long as you give appropriate credit to the original author(s) and the source, provide a link to the Creative Commons licence, and indicate if changes were made. The images or other third party material in this article are included in the article's Creative Commons licence, unless indicated otherwise in a credit line to the material. If material is not included in the article's Creative Commons licence and your intended use is not permitted by statutory regulation or exceeds the permitted use, you will need to obtain permission directly from the copyright holder. To view a copy of this licence, visit <http://creativecommons.org/licenses/by/4.0/>.

References

1. <http://j-parc.jp/MatLife/en/index.html>, J-PARC
2. <http://neutrons.ornl.gov/facilities/SNS/>, SNS
3. <http://europespallationsource.se>, European Spallation Source ESS ERIC
4. S. Peggs, Ess technical design report- (ess-2013-0001). <http://eval.esss.lu.se/cgi-bin/public/DocDB/ShowDocument?docid=274>
5. R. Garoby, The European spallation source design. *Phys. Scr.* **93**(1), 014001 (2018)
6. M. Lindroos, S. Bousson, R. Calaga, H. Danared, G. Devanz, R. Duperrier, J. Eguia, M. Eshraqi, S. Gammino, H. Hahn, A. Jansson, C. Oyon, S. Pape-Moller, S. Peggs, A. Ponton, K. Rathsmann, R. Ruber, T. Satogata, G. Trahern, The European spallation source. *Nucl. Instrum. Methods Phys. Res. Sect. B: Beam Interact. Mater. Atoms* **269**(24), 3258–3260 (2011)
7. F. Mezei, New perspectives from new generations of neutron sources. *C.R. Phys.* **8**(7), 909–920 (2007)
8. C. Vettier, C.J. Carlile, P. Carlsson, Progress for the European spallation source in Scandinavia. *Nucl. Instrum. Methods Phys. Res., Sect. A* **600**(1), 8–9 (2009)
9. K. Andersen, D. Argyriou, A. Jackson, J. Houston, P. Henry, P. Deen, R. Toft-Petersen, P. Beran, M. Strobl, T. Arnold, H. Wacklin-Knecht, N. Tsapatsaris, E. Oksanen, R. Woracek, W. Schweika, D. Mannix, A. Hiess, S. Kennedy, O. Kirstein, S.P. Årsköld, J. Taylor, M. Hagen, G. Laszlo, K. Kanaki, F. Piscitelli, A. Khaplanov, I. Stefanescu, T. Kittelmann, D. Pfeiffer, R. Hall-Wilton, C. Lopez, G. Aprigliano, L.

- Whitelegg, F. Moreira, M. Olsson, H. Bordallo, D. Martín-Rodríguez, H. Schneider, M. Sharp, M. Hartl, G. Nagy, S. Ansell, S. Pullen, A. Vickery, A. Fedrigo, F. Mezei, M. Arai, R. Heenan, W. Halcrow, D. Turner, D. Raspino, A. Orszulik, J. Cooper, N. Webb, P. Galsworthy, J. Nightingale, S. Langridge, J. Elmer, H. Frielinghaus, R. Hanslik, A. Gussen, S. Jaksch, R. Engels, T. Kozielowski, S. Butterweck, M. Feyngenson, P. Harbott, A. Poqué, A. Schwaab, K. Lieutenant, N. Violini, J. Voigt, T. Brückel, M. Koenen, H. Kämmerling, E. Babcock, Z. Salhi, A. Wischnewski, A. Heynen, S. Désert, J. Jestin, F. Porcher, X. Fabrèges, G. Fabrèges, B. Annighöfer, S. Klimko, T. Dupont, T. Robillard, A. Goukassov, S. Longeville, C. Alba-Simionesco, P. Bourges, J.G.L. Bouffy, P. Lavie, S. Rodrigues, E. Calzada, M. Lerche, B. Schillinger, P. Schmakat, M. Schulz, M. Seifert, W. Lohstroh, W. Petry, J. Neuhaus, L. Loaiza, A. Tartaglione, A. Glavic, S. Schütz, J. Stahn, E. Lehmann, M. Morgano, J. Scheffer, U. Filges, C. Klausner, C. Niedermayer, J. Fenske, G. Nowak, M. Rouijaa, D. Siemers, R. Kiehn, M. Müller, H. Carlsen, L. Udby, K. Lefmann, J. Birk, S. Holm-Dahlin, M. Bertelsen, U.B. Hansen, M. Olsen, M. Christensen, K. Iversen, N. Christensen, H. Rønnow, P. Freeman, B. Hauback, R. Kolevatov, I. Llamas-Jansa, A. Orecchini, F. Sacchetti, C. Petrillo, A. Paciaroni, P. Tozzi, M. Zanatta, P. Luna, I. Herranz, O. del Moral, M. Huerta, M. Magán, M. Mosconi, E. Abad, J. Aguilar, S. Stepanyan, G. Bakedano, R. Vivanco, I. Bustinduy, F. Sordo, J. Martínez, R. Lechner, F. Villacorta, J. Šaroun, P. Lukáš, M. Markó, M. Zanetti, S. Bellissima, L. del Rosso, F. Masi, C. Bovo, M. Chowdhury, A.D. Bonis, L.D. Fresco, C. Scatigno, S. Parker, F. Fernandez-Alonso, D. Colognesi, R. Senesi, C. Andreani, G. Gorini, G. Scionti, A. Schreyer, The instrument suite of the European spallation source. Nucl. Instrum. Methods Phys. Res., Sect. A **957**, 163402 (2020)
10. D.P. Hoogerheide, F. Heinrich, B.B. Maranville, C.F. Majkrzak, Accurate background correction in neutron reflectometry studies of soft condensed matter films in contact with fluid reservoirs. *J. Appl. Crystallogr.* **53**, 15–26 (2020)
 11. J. Stahn, A. Glavic, Focusing neutron reflectometry: implementation and experience on the TOF-reflectometer Amor, *Nuclear Instruments and Methods in Physics Research Section A: Accelerators, Spectrometers, Detectors and Associated Equipment*, vol. 821, no. Supplement C, pp. 44–54, (2016)
 12. R.A. Campbell, H.P. Wacklin, I. Sutton, R. Cubitt, G. Fragneto, FIGARO: the new horizontal neutron reflectometer at the ILL. *Euro. Phys. J. Plus* **126**(11), 1–22 (2011)
 13. R. Bewley, J. Taylor, S. Bennington, LET, a cold neutron multi-disk chopper spectrometer at ISIS. *Nucl. Instrum. Methods Phys. Res., Sect. A* **637**(1), 128–134 (2011)
 14. N. Cherkashyna, K. Kanaki, T. Kittelmann, U. Filges, P. Deen, K. Herwig, G. Ehlers, G. Greene, J. Carpenter, R. Connatser, R. Hall-Wilton, P.M. Bentley, High energy particle background at neutron spallation sources and possible solutions. *J. Phys: Conf. Ser.* **528**, 012013 (2014)
 15. K. Zeitelhack, Search for alternative techniques to helium-3 based detectors for neutron scattering applications. *Neutron News* **23**(4), 10–13 (2012)
 16. A.J. Hurd, R.T. Kouzes, Why new neutron detector materials must replace helium-3. *Euro. Phys. J. Plus* **129**(10), 1–3 (2014)
 17. <http://www.icnd.org>, International collaboration on the development of neutron detectors
 18. A. Cho, Helium-3 shortage could put freeze on low-temperature research. *Science* **326**(5954), 778–779 (2009)
 19. U. G. A. Office, Neutron detectors: alternatives to using Helium-3, Technical Report. GAP-11-753, U.S. Government Accountability Office, (September 2011)
 20. D. Kramer, For some, helium-3 supply picture is brightening. *Phys. Today* **64**, 20–23 (2011)
 21. D. A. Shea, D. Morgan, The helium-3 shortage: supply, demand, and options for congress, *Congressional Research Service*, (2010)
 22. C. Höglund, J. Birch, K. Andersen, T. Bigault, J.-C. Buffet, J. Correa, P. van Esch, B. Guerard, R. Hall-Wilton, J. Jensen, A. Khaplanov, F. Piscitelli, C. Vettier, W. Vollenberg, L. Hultman, B4C thin films for neutron detection. *J. Appl. Phys.* **111**(10), 104908 (2012)
 23. C. Höglund, K. Zeitelhack, P. Kudejova, J. Jensen, G. Greczynski, J. Lu, L. Hultman, J. Birch, R. Hall-Wilton, Stability of 10B4C thin films under neutron radiation. *Radiat. Phys. Chem.* **113**, 14–19 (2015)
 24. S. Schmidt, C. Höglund, J. Jensen, L. Hultman, J. Birch, R. Hall-Wilton, Low-temperature growth of boron carbide coatings by direct current magnetron sputtering and high-power impulse magnetron sputtering. *J. Mater. Sci.* **51**(23), 10418–10428 (2016)
 25. M. Anastasopoulos, R. Bebb, K. Berry, J. Birch, T. Bryś, J.-C. Buffet, J.-F. Clergeau, P. Deen, G. Ehlers, P. van Esch, S. Everett, B. Guerard, R. Hall-Wilton, K. Herwig, L. Hultman, C. Höglund, I. Iruretagoiena, F. Issa, J. Jensen, A. Khaplanov, O. Kirstein, I.L. Higuera, F. Piscitelli, L. Robinson, S. Schmidt, I. Stefanescu, Multi-Grid detector for neutron spectroscopy: results obtained on time-of-flight spectrometer CNCS. *J. Instrum.* **12**(04), P04030 (2017)
 26. J. Birch, J.-C. Buffet, J.-F. Clergeau, J. Correa, P. van Esch, M. Ferraton, B. Guerard, J. Halbwachs, R. Hall-Wilton, L. Hultman, C. Höglund, A. Khaplanov, M. Koza, F. Piscitelli, M. Zbiri, In-beam test of the

- Boron-10 multi-grid neutron detector at the IN6 time-of-flight spectrometer at the ILL. *J. Phys: Conf. Ser.* **528**(1), 012040 (2014)
27. J. Birch, J.C. Buffet, J. Correa, P. van Esch, B. Guérard, R. Hall-Wilton, C. Höglund, L. Hultman, A. Khaplanov, F. Piscitelli, 10B4C multi-grid as an alternative to ^3He for large area neutron detectors. *IEEE Trans. Nucl. Sci.* **60**, 871–878 (2013)
 28. B. Guerard, J. Buffet, Ionizing radiation detector - patent no. 20110215251., Sept. 8 2011. US Patent App. 13/038,915
 29. F. Piscitelli, Novel boron-10-based detectors for neutron scattering science. *Euro. Phys. J. Plus* **130**(2), 1–9 (2015)
 30. F. Piscitelli, G. Mauri, F. Messi, M. Anastasopoulos, T. Arnold, A. Glavic, C. Höglund, T. Ilves, I.L. Higuera, P. Pazmandi, D. Raspino, L. Robinson, S. Schmidt, P. Svensson, D. Varga, R. Hall-Wilton, Characterization of the multi-blade 10B-based detector at the CRISP reflectometer at ISIS for neutron reflectometry at ESS. *J. Instrum.* **13**(05), P05009 (2018)
 31. F. Piscitelli, J.C. Buffet, J.F. Clergeau, S. Cuccaro, B. Guérard, A. Khaplanov, Q.L. Manna, J.M. Rigal, P.V. Esch, Study of a high spatial resolution 10 B -based thermal neutron detector for application in neutron reflectometry: the multi-blade prototype. *J. Instrum.* **9**(03), P03007 (2014)
 32. F. Piscitelli, F. Messi, M. Anastasopoulos, T. Brys, F. Chicken, E. Dian, J. Fuzi, C. Höglund, G. Kiss, J. Orban, P. Pazmandi, L. Robinson, L. Rosta, S. Schmidt, D. Varga, T. Zsiros, R. Hall-Wilton, The multi-blade Boron-10-based neutron detector for high intensity neutron reflectometry at ESS. *J. Instrum.* **12**(03), P03013 (2017)
 33. F. Piscitelli, J. C. Buffet, J. Correa, P. V. Esch, B. Guérard, and A. Khaplanov, Study of a 10b-based multi-blade detector for neutron scattering science, in *Conference record of Nuclear Science Symposium and Medical Imaging Conference (NSS/MIC) Anaheim* (I. T. N. Sci., ed.), pp. 171–175, (2012)
 34. F. Piscitelli, *Boron-10 layers, neutron reflectometry and thermal neutron gaseous detectors*. Ph. D. thesis, Institut Laue-Langevin and University of Perugia, (2014) - [arXiv:1406.3133](https://arxiv.org/abs/1406.3133)
 35. G. Mauri, F. Messi, M. Anastasopoulos, T. Arnold, A. Glavic, C. Höglund, T. Ilves, I. Lopez Higuera, P. Pazmandi, D. Raspino, L. Robinson, S. Schmidt, P. Svensson, D. Varga, R. Hall-Wilton, and F. Piscitelli, “Neutron reflectometry with the Multi-Blade 10B-based detector, in *Proceedings of the Royal Society of London A: Mathematical, Physical and Engineering Sciences*, vol. 474, no. 2216, (2018)
 36. M. Henske, M. Klein, M. Köhli, P. Lennert, G. Modzel, C. Schmidt, U. Schmidt, The 10B based Jalousie neutron detector—an alternative for ^3He filled position sensitive counter tubes. *Nucl. Instrum. Methods Phys. Res., Sect. A* **686**, 151–155 (2012)
 37. G. Modzel, M. Henske, A. Houben, M. Klein, M. Köhli, P. Lennert, M. Meven, C. Schmidt, U. Schmidt, W. Schweika, Absolute efficiency measurements with the 10b based jalousie detector. *Nucl. Instrum. Methods Phys. Res., Sect. A* **743**, 90–95 (2014)
 38. G. Albani, E.P. Cippo, G. Croci, A. Muraro, E. Schooneveld, A. Scherillo, R. Hall-Wilton, K. Kanaki, C. Höglund, L. Hultman, J. Birch, G. Claps, F. Murtas, M. Rebai, M. Tardocchi, G. Gorini, Evolution in boron-based GEM detectors for diffraction measurements: from planar to 3D converters. *Meas. Sci. Technol.* **27**(11), 115902 (2016)
 39. G. Croci et al., Diffraction measurements with a boron-based GEM neutron detector. *EPL* **107**(1), 12001 (2014)
 40. A. Athanasiades, N. N. Shehad, C. S. Martin, L. Sun, and J. L. Lacy, Straw detector for high rate, high resolution neutron imaging, in *IEEE Nuclear Science Symposium Conference Record, 2005*, vol. 2, pp. 623–627, (2005)
 41. J. L. Lacy, L. Sun, C. S. Martin, A. Athanasiades, and T. D. Lyons, One meter square high rate neutron imaging panel based on boron straws, in *2009 IEEE Nuclear Science Symposium Conference Record (NSS/MIC)*, pp. 1117–1121, (2009)
 42. J.L. Lacy, A. Athanasiades, N.N. Shehad, R.A. Austin, C.S. Martin, Novel neutron detector for high rate imaging applications. *IEEE NSS, Norfolk* **1**, 392–396 (2002)
 43. J. Lacy, Performance of 1 meter straw detector for high rate neutron imaging. in *IEEE Nuclear Science Symposium Conference Record*, 20–26 (2006)
 44. J. L. Lacy, A. Athanasiades, L. Sun, C. S. Martin, T. D. Lyons, M. A. Foss, and H. B. Haygood, Boron-coated straws as a replacement for ^3He -based neutron detectors, *Nuclear Instruments and Methods in Physics Research Section A: Accelerators, Spectrometers, Detectors and Associated Equipment*, vol. 652, no. 1, pp. 359 – 363, 2011. Symposium on Radiation Measurements and Applications (SORMA) XII (2010)
 45. J.L. Lacy, A. Athanasiades, C.S. Martin, L. Sun, G.L. Vazquez-Flores, The evolution of neutron straw detector applications in homeland security. *IEEE Trans. Nucl. Sci.* **60**(2), 1140–1146 (2013)

46. M. Köhli, F. Allmendinger, W. Häußler, T. Schröder, M. Klein, M. Meven, U. Schmidt, Efficiency and spatial resolution of the CASCADE thermal neutron detector. *Nucl. Instrum. Methods Phys. Res., Sect. A* **828**, 242–249 (2016). 8
47. M. Klein and C. J. Schmidt, CASCADE, neutron detectors for highest count rates in combination with ASIC/FPGA based readout electronics, *Nuclear Instruments and Methods in Physics Research Section A: Accelerators, Spectrometers, Detectors and Associated Equipment*, vol. 628, no. 1, pp. 9–18, (2011). VCI 2010 Proceedings of the 12th International Vienna Conference on Instrumentation
48. F. Sauli, Gem: a new concept for electron amplification in gas detectors. *Nucl. Instrum. Methods Phys. Res., Sect. A* **386**(2), 531–534 (1997)
49. D. Pfeiffer, F. Resnati, J. Birch, M. Etxegarai, R. Hall-Wilton, C. Höglund, L. Hultman, I. Llamas-Jansa, E. Oliveri, E. Oksanen, L. Robinson, L. Ropelewski, S. Schmidt, C. Strelci, P. Thuiner, First measurements with new high-resolution gadolinium-GEM neutron detectors. *J. Instrum.* **11**(05), P05011 (2016)
50. D. Pfeiffer, F. Resnati, J. Birch, R. Hall-Wilton, C. Höglund, L. Hultman, G. Iakovidis, E. Oliveri, E. Oksanen, L. Ropelewski, P. Thuiner, The μ TPC method: improving the position resolution of neutron detectors based on MPGDs. *J. Instrum.* **10**(04), P04004 (2015)
51. R. Schulte, F. Swanson, M. Kesselman, The use of large area silicon sensors for thermal neutron detection. *Nucl. Instrum. Methods Phys. Res., Sect. A* **353**(1), 123–127 (1994)
52. A. Miresghhi, G. Cho, J. Drewery, T. Jing, S.N. Kaplan, V. Perez-Mendez, D. Wildermuth, Amorphous silicon position sensitive neutron detector. *IEEE Trans. Nucl. Sci.* **39**, 635–640 (1992)
53. C. Petrillo, F. Sacchetti, O. Toker, N. Rhodes, Solid state neutron detectors. *Nucl. Instrum. Methods Phys. Res., Sect. A* **378**(3), 541–551 (1996)
54. G. Mauri, M. Mariotti, F. Casinini, F. Sacchetti, C. Petrillo, Development of pulse shape analysis for noise reduction in Si-based neutron detectors. *Nucl. Instrum. Methods Phys. Res., Sect. A* **910**, 184–193 (2018)
55. A. Khaplanov, F. Piscitelli, J.C. Buffet, J.F. Clergeau, J. Correa, P. van Esch, M. Ferraton, B. Guerard, R. Hall-Wilton, Investigation of gamma-ray sensitivity of neutron detectors based on thin converter films. *J. Instrum.* **8**(10), P10025 (2013)
56. G. Mauri, F. Messi, K. Kanaki, R. Hall-Wilton, E. Karnickis, A. Khaplanov, and F. Piscitelli, Fast neutron sensitivity of neutron detectors based on Boron-10 converter layers, *J. Instrum.*, vol. 13, no. 03, p. P03004 ([arxiv:1712.05614](https://arxiv.org/abs/1712.05614)), (2018)
57. G. Mauri, F. Messi, K. Kanaki, R. Hall-Wilton, F. Piscitelli, Fast neutron sensitivity for ^3He detectors and comparison with Boron-10 based neutron detectors. *EPJ Tech. Instrum.* **6**(1), 3 (2019). [arxiv:1902.09870](https://arxiv.org/abs/1902.09870)
58. G. Knoll, *Radiation Detection and Measurement*, third edn. (Wiley, Hoboken, 2000)
59. M. Manolopoulou, M. Fragopoulou, S. Stoulos, E. Vagena, W. Westmeier, M. Zamani, Neutron spectrometry with He-3 proportional counters. *J. Phys: Conf. Ser.* **366**, 012033 (2012)
60. T. Iijima, T. Mukaiyama, K. Shirakata, Measurement of fast neutron spectrum with helium-3 proportional counter. *J. Nucl. Sci. Technol.* **8**(4), 192–200 (1971)
61. L. Swiderski, M. Moszynski, D. Wolski, J. Iwanowska, T. Szczesniak, G. Pausch, C. Plettner, J. Stein, P. Schotanus, and C. Hurlbut, Comparison of neutron detection efficiency using a he-3 counter and a boron-10 loaded liquid scintillator ej309b5, in *2009 IEEE Nuclear Science Symposium Conference Record (NSS/MIC)*, pp. 892–897, (2009)
62. T.J. Langford, E.J. Beise, H. Breuer, C.R. Heimbach, G. Ji, J.S. Nico, Development and characterization of a high sensitivity segmented fast neutron spectrometer (fans-2). *J. Instrum.* **11**(01), P01006 (2016)
63. Yinong Liang, Ting Zhu, Andreas Enqvist, Timing characterization of helium-4 fast neutron detector with ej-309 organic liquid scintillator. *EPJ Web Conf.* **170**, 07005 (2018)
64. <https://www.arctisdetectors.com> , Arktis detectors
65. R. Jebali, J. Scherzinger, J. Annand, R. Chandra, G. Davatz, K. Fissum, H. Friederich, U. Gendotti, R. Hall-Wilton, E. Håkansson, K. Kanaki, M. Lundin, D. Murer, B. Nilsson, A. Rosborg, H. Svensson, A first comparison of the responses of a ^4He -based fast-neutron detector and a ne-213 liquid-scintillator reference detector. *Nucl. Instrum. Methods Phys. Res., Sect. A* **794**, 102–108 (2015)
66. <https://www.nndc.bnl.gov/sigma/> , NIST National Nuclear Data Center–Evaluated Nuclear Data File – ENDF/B-VII.1 (USA, 2011) database
67. M. Chadwick, M. Herman, P. Obložinský, M. Dunn, Y. Danon, A. Kahler, D. Smith, B. Pritychenko, G. Arbanas, R. Arcilla, R. Brewer, D. Brown, R. Capote, A. Carlson, Y. Cho, H. Derrien, G. Guber, G. Hale, S. Hoblit, S. Holloway, T. Johnson, T. Kawano, B. Kiedrowski, H. Kim, S. Kunieda, N. Larson, L. Leal, J. Lestone, R. Little, E. McCutchan, R. MacFarlane, M. MacInnes, C. Mattoon, R. McKnight, S. Mughabghab, G. Nobe, G. Palmiotti, A. Palumbo, M. Pigni, V. Pronyaev, R. Sayer, A. Sonzogni, N. Summers, P. Talou, I. Thompson, A. Trkov, R. Vogt, S. [van der Marck], A. Wallner, M. White, D. Wiarda, and P. Young, “ENDF/B-VII.1 Nuclear Data for Science and Technology: Cross Sections, Covariances, Fission Product Yields and Decay Data,” *Nucl. Data Sheets*, vol. 112, no. 12, pp. 2887–2996, (2011). Special Issue on ENDF/B-VII.1 Library

68. J.F. Ziegler, RBS/ERD simulation problems: stopping powers, nuclear reactions and detector resolution. Nucl. Instrum. Methods Phys. Res. B **136**, 141–146 (1998)
69. J.F. Ziegler, M.D. Ziegler, J.P. Biersack, SRIM—the stopping and range of ions in matter (2010). Nucl. Instrum. Methods Phys. Res. B **268**, 1818–1823 (2010)
70. <https://etd.canon/en/index.html> , Toshiba-CANON etd detectors
71. <https://www.industrial.ai/measurement-sensing/radiationmeasurement> , Reuter-Stokes detectors
72. <http://www.cremat.com>, Cremat inc - electronics for pulse detection
73. <http://www.caen.it> , CAEN - Electronic Instrumentation
74. F. Messi, H. Perrey, K. Fissum, M. Akkawi, R. A. Jebali, J. Annand, P. Bentley, L. Boyd, C. Cooper-Jensen, D. DiJulio, J. Freitas-Ramos, R. Hall-Wilton, A. Huusko, T. Ilves, F. Issa, A. Jalgen, K. Kanaki, E. Karnickis, A. Khaplanov, S. Koufigar, V. Maulerova, G. Mauri, N. Mauritzson, W. Pei, F. Piscitelli, E. Rofors, J. Scherzinger, H. Soderhielm, D. Soderstrom, and I. Stefanescu, The neutron tagging facility at Lund University, [arXiv:1711.10286](https://arxiv.org/abs/1711.10286) (submitted to IAEA Technical Report on Modern Neutron Detection (2017)), (2017)
75. J. Scherzinger, J. Annand, G. Davatz, K. Fissum, U. Gendotti, R. Hall-Wilton, E. Håkansson, R. Jebali, K. Kanaki, M. Lundin, B. Nilsson, A. Rosborge, H. Svensson, Tagging fast neutrons from an $^{241}\text{Am}/^9\text{Be}$ source. Appl. Radiat. Isot. **98**, 74–79 (2015)
76. Calibration certified at the radiochemical centre, amersham, england hp7 9ll on 3 september, (1973)
77. J. Scherzinger, R.A. Jebali, J. Annand, K. Fissum, R. Hall-Wilton, N. Koufigar, N. Mauritzson, F. Messi, H. Perrey, E. Rofors, A comparison of untagged gamma-ray and tagged-neutron yields from $^{241}\text{AmBe}$ and $^{238}\text{PuBe}$ sources. Appl. Radiat. Isot. **127**, 98–102 (2017)
78. A.G. Kovlov et al., translated from Atomnaya Energiya 25 (1968) 534
79. A.C. Overholt, A.L. Melott, D. Atri, Modeling cosmic ray proton induced terrestrial neutron flux: a look-up table. J. Geophys. Res. Space Phys. **118**(6), 2765–2770 (2013)
80. B. Wiegel and A. Alevra, NEMUS-the PTB neutron multisphere spectrometer: Bonner spheres and more, nuclear instruments and methods in Physics Research Section A: accelerators, spectrometers, detectors and associated equipment, 476(1), pp. 36–41, *Int* (Workshop on Neutron Field Spectrometry in Science, Technology and Radiation Protection, 2002)
81. Physikalisch-Technische Bundesanstalt (PTB) - Measurements of Neutron Spectra Induced by Cosmic Radiation at Altitudes of 85 m, 1195 m and 2650 m https://www.ptb.de/cms/en/ptb/fachabteilungen/abt6/forschungsnachrichtenabt6/news-from-the-annual-report.html?tx_news_pi1%5Bnews%5D=4592&tx_news_pi1%5Bcontroller%5D=News&tx_news_pi1%5Baction%5D=detail&tx_news_pi1%5Bday%5D=4&tx_news_pi1%5Bmonth%5D=1&tx_news_pi1%5Byear%5D=2010&cHash=0f14a71bf7592050c1fc01e1cf8c71c0, 2010
82. A. Zimbal, A. Kasper, M. Reginatto, H. Schuhmacher, and B. Wiegel, Measurements of neutron energy spectra at altitudes of 85 m, 1195 m and 2650 m, in *Contrib. to the 11th Neutron and Ion Dosimetry Symposium (NEUDOS-11)*, iThemba LABS, Cape Town, South Africa, 12 - 16 October 2009
83. K. Zeitelhack, Cosmic neutron rates at the FRM-II reactor. (Private communication)